A&A 370, 570–575 (2001)
DOI: 10.1051/0004-6361:20010253

Astronomy & Astrophysics

Observations of the supernova remnant G54.1+0.3: X-ray spectrum and evidence for an X-ray jet

F. J. Lu[1,2], B. Aschenbach[1], and L. M. Song[2]

[1] Max-Planck-Institut für Extraterrestrische Physik, Giessenbachstrasse, 85748 Garching bei München, Germany
[2] Laboratory of Cosmic Ray and High Energy Astrophysics, Institute of High Energy Physics, CAS, Beijing 100039, China

Received 16 May 2000 / Accepted 15 February 2001

Abstract. We present analyses of the *ROSAT* PSPC and the *ASCA* SIS and GIS observations of the Crab-like supernova remnant (SNR) G54.1+0.3. The spectrum is best fitted by a power law model with a photon index of $-1.9^{+0.2}_{-0.2}$, absorbed energy flux of 6.8 10^{-12} erg cm^{-2} s^{-1} in the 0.7–10 keV band, and a column density of $17.9^{+2.8}_{-2.5}$ 10^{21} cm^{-2}. The high absorption column density indicates a distance close to the radius of the galaxy. The 0.7–10.0 keV X-ray luminosity of G54.1+0.3 is 1.4 $10^{35} d_{10}^2$ erg s^{-1}, where d_{10} is the distance in 10 kpc. With an image restoration method, we have deconvolved the X-ray image of the remnant. There is evidence for an X-ray jet pointing to the north-east with a length of about 40″ measured from the center of the nebula. Its X-ray luminosity in the 0.1–2.4 keV range is about 2.1 $10^{34} d_{10}^2$ erg s^{-1}. The X-ray jet is consistent with the radio extension of G54.1+0.3 to the north-east in both direction and position.

Key words. X-ray: ISM – ISM: supernova remnants – ISM: jet and outflows – ISM: individual: G54.1+0.3

1. Introduction

The radio source G54.1+0.3 was first suggested to be a Crab-like SNR by Reich et al. (1985) for its flat spectral index of $\alpha \sim -0.1 \pm 0.1$, filled-center morphology and significant polarization. This classification of G54.1+0.3 was confirmed by Velusamy & Becker (1988) with high resolution multifrequency observations using the VLA and OSRT. In the high resolution VLA maps, G54.1+0.3 has a filled-center brightness distribution which peaks around $\alpha_{2000} = 19^{\rm h}30^{\rm m}30\overset{\rm s}{.}0$, $\delta_{2000} = 18°52'11''$ and extensions to the north-east and north (Velusamy & Becker 1988). They pointed out that these extensions are reminiscent of the radio jets seen in the Crab (Velusamy 1984), CTB80 (Angerhofer et al. 1981) and G332.4+0.1 (Roger et al. 1985).

X-rays from G54.1+0.3 were detected by the *EINSTEIN* IPC (resolution $\sim 1'$) with a source strength of 0.016 ± 0.004 counts s^{-1} in the energy band 0.5–4.0 keV (Seward 1989). No extent of the X-ray emission was found, due to both its small angular size ($2.0' \times 1.2'$) (Velusamy & Becker 1988) and its low flux. A power law spectral fitting with energy index of 1.0 gave a column density, $N_{\rm H}$, between 5 10^{21} and 1 10^{23} cm^{-2}, with the best fit value of 3 10^{22} cm^{-2}, indicating a large distance.

Send offprint requests to: F. J. Lu,
e-mail: lufj@astrosv1.ihep.ac.cn

Here we present the analyses of the *ROSAT* PSPC and the *ASCA* GIS and SIS observations of G54.1+0.3. We obtain spectral information, and, with the aid of an image restoration method, we create a high spatial resolution X-ray map of the remnant which shows evidence for an X-ray jet pointing to the north-east.

2. Observations and analysis method

The *ROSAT* PSPC pointing observation of SNR G54.1+0.3 was carried out from April 11 to 18, 1991 with a total acceptable observational time of 20 271 s. We have used *EXSAS* (Zimmermann et al. 1998) to analyze the spectrum and produced a 0.1–2.5 keV X-ray image (Fig. 1) with a spatial resolution comparable to the intrinsic resolution of the PSPC (40″).

G54.1+0.3 was also observed with the *ASCA* observatory (Tanaka et al. 1994) continuously from April 27 to 28, 1997, using the two Gas Imaging Spectrometers (GIS-2 and GIS-3) and the two Solid State Imaging Spectrometers (SIS-0 and SIS-1). Data were collected by the two GIS detectors with a photon time-of-arrival resolution of 4.88 10^{-4} s in the high bit-rate modes. An effective exposure time of 16.5 ks was achieved for each detector. The SIS detectors were operated in the 1-CCD faint mode in which read-out is every 4 s. All the SIS data were filtered using the standard screening criteria, which resulted in

effective exposures of 19 ks and 20.7 ks for SIS-0 and SIS-1, respectively. Since the two GIS detectors were operated in the high time-of-arrival resolution mode, we used the GIS data for temporal analysis. The SIS detectors which are sensitive to photons in the range 0.5–10.0 keV have superior energy resolution compared to the GIS, and so the SIS data are used for spectral analysis.

Due to the small angular size ($120'' \times 75''$) of G54.1+0.3 and the limited spatial resolution ($\sim 40''$) of the PSPC, the PSPC observation cannot directly give an even coarsely resolved image of G54.1+0.3. In order to obtain an image with higher spatial resolution, we applied the widely used Lucy-Richardson formalism (Richardson 1972; Lucy 1974) to eliminate the point spread function effect in Fig. 1. In the iteration process we have used the mean background as the lower limit constraint, in order to improve the quality of the restored image, as suggested by Li & Wu (1994), Lu et al. (1996) and Zhang et al. (1998).

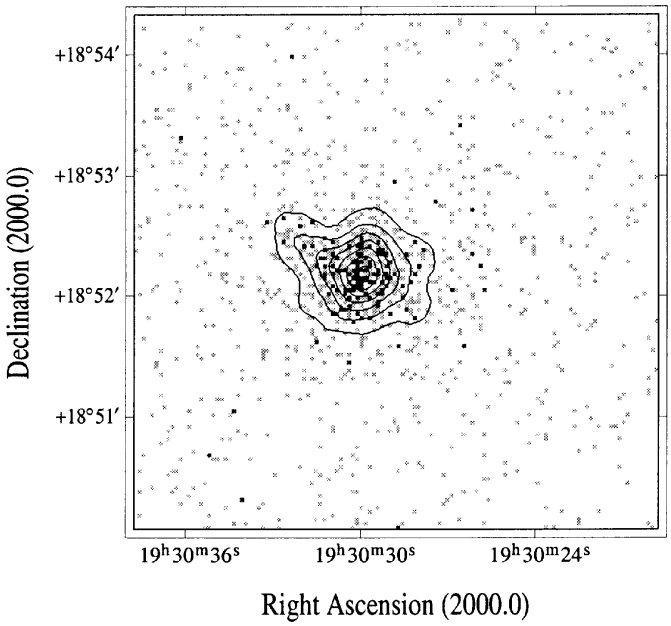

Fig. 1. Count-rate map in the 0.1–2.5 keV range obtained from the *ROSAT* PSPC observation of G54.1+0.3. The contours overlaid represent the count-rate map smoothed with a $10''$ *FWHM* Gaussian filter. The contour intervals are linear in steps of 10^{-5} counts s^{-1} per $2'' \times 2''$ pixel. The lowest contour corresponds to a brightness level of 10^{-5} counts s^{-1} per pixel

3. Results

3.1. Spectrum

The *ASCA* SISs data were used to investigate the spectrum of G54.1+0.3. Photons used were extracted from a 4.5 arcmin radius region. After subtracting the source region, another region of the CCD was used for background subtraction. The source and background spectra obtained from both the SISs were added to improve the statistics. The spectral analysis software is XSPEC. Counts with energies above 8 keV were discarded because of the poor signal to noise ratio. We have tried power law, blackbody, single temperature bremsstrahlung and Raymond-Smith thermal plasma (Raymond & Smith 1977) models to fit the spectrum, and found that only the power law model and the thermal bremsstrahlung model give statistically acceptable and reasonable fits. The obtained parameters of the power law model are: photon index = $\alpha - 1.9^{+0.2}_{-0.2}$, column density = $N_{\rm H}$ $17.9^{+2.8}_{-2.5}$ 10^{21} cm^{-2}, absorbed 0.7–10.0 keV energy flux = 6.8 10^{-12} erg cm^{-2} s^{-1}, unabsorbed 0.7–10.0 keV energy flux = 1.14 10^{-11} erg cm^{-2} s^{-1}, reduced $\chi^2 = 0.7$. Parameters of a thermal bremsstrahlung model are: temperature $kT_{\rm e} = 7.9^{+3.9}_{-3.1}$ keV, column density $N_{\rm H} = 15.4^{+2.0}_{-1.9}$ 10^{21} cm^{-2}, absorbed 0.7–10.0 keV energy flux = 8.8 10^{-12} erg cm^{-2} s^{-1}, reduced $\chi^2 = 0.8$. We choose the power law model in this paper as it has the smallest χ^2 and a power law X-ray spectrum is typical for the X-ray emission of a Crab-like SNR. For illustration, we show in Fig. 2 the best fit power law model and the residuals.

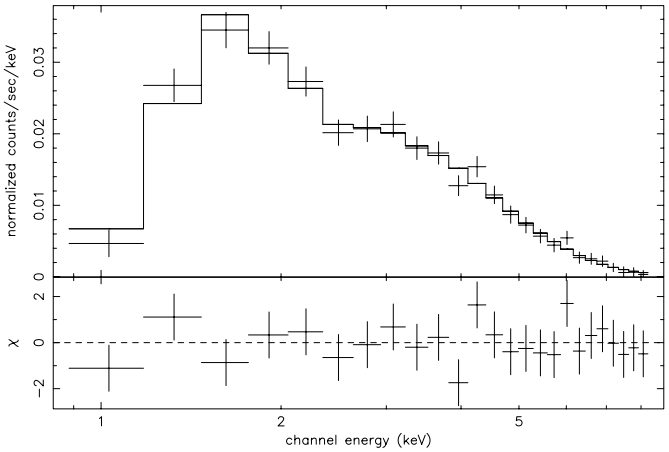

Fig. 2. Spectral fitting results to the X-ray emission of G54.1+0.3 obtained by the *ASCA* SIS with a power law model. Model parameters are given in the text

We have also analyzed the *ROSAT* PSPC data for the spectrum of G54.1+0.3. The fits are consistent with the *ASCA* SIS result. The power law model yields a photon index of -0.8 with a 1σ error range of -2.8 to 0.0 and an absorption column density of 12.3 10^{21} cm^{-2} with a 1σ error range of 8 to 20 10^{21} cm^{-2}. Figure 3 shows the error ranges of the photon index and the absorption column density of a power law model fitted to the PSPC data. The 1σ error ranges of the photon index and absorption column density derived from the fits to the *ASCA* SIS data are indicated by the cross.

3.2. Temporal analysis

In order to examine the *ASCA* GIS data for temporal variability we have extracted photons from a 6 arcmin radius circle centered on G54.1+0.3. A search for regular

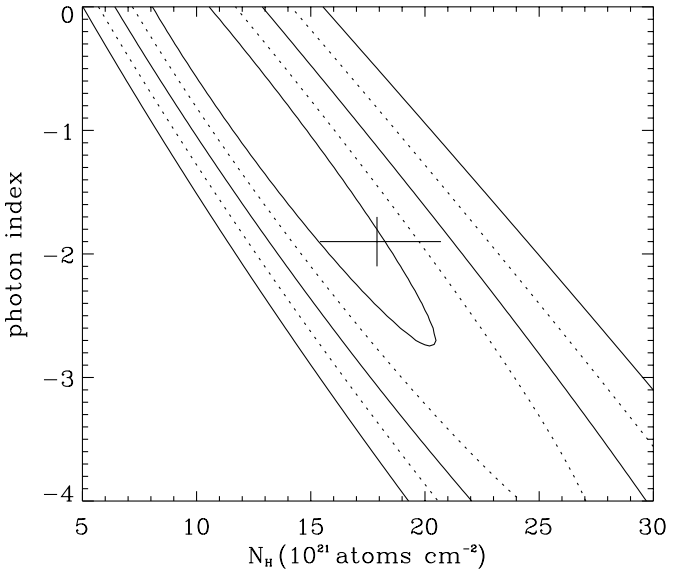

Fig. 3. χ^2 confidence contours on the column density–photon index plane of the power law spectral fitting of the *ROSAT* PSPC observation of G54.1+0.3. Contours are in steps of 1σ running from 1σ to 5σ. The cross denotes the results derived from *ASCA* SIS data

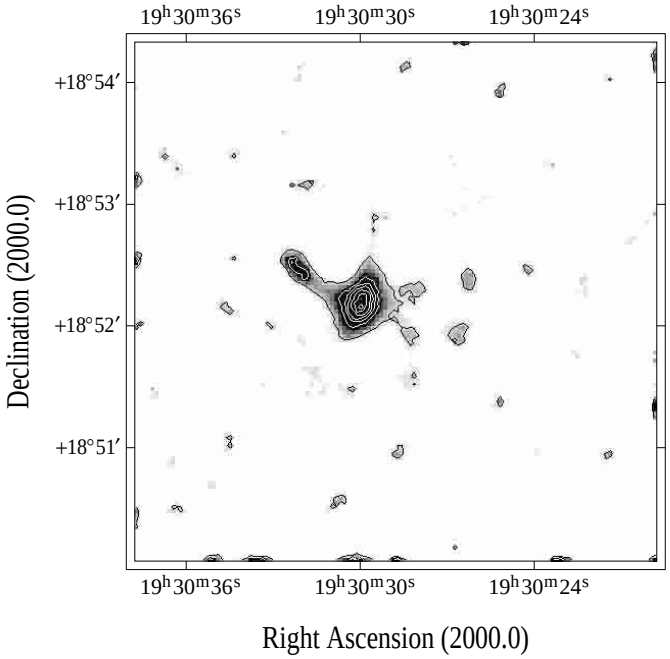

Fig. 4. Restored 0.1–2.5 keV X-ray brightness map of G54.1+0.3. The contour intervals are linear with a step size of 4 10^{-5} count s^{-1} per $2'' \times 2''$ pixel. The lowest contour corresponds to a brightness level of 2 10^{-5} count s^{-1} per pixel

pulsations from the source was made by combining the two GIS high-time-resolution data sets (time resolution 4.88 10^{-4} s); the arrival times of a total of 1805 counts were barycentered. A restricted search for periodic signals between 0.01 s and 2 s using a folding technique (20 phase bins per period) was performed. Taking into account the total number of trials, we have not detected any pulsation with a significance of more than 3σ in this period range. The upper limit of a pulsed fraction is 31% with a confidence of 90%.

3.3. Image restoration results

The spectral distribution of photons detected by the *ROSAT* PSPC peaks at 1.5 keV and is quite symmetric. We thus use the PSPC point spread function at 1.5 keV and the method described in Sect. 2 to restore the original image (cf. Fig. 1). The restoration process stops after 50 iterations (indeed, the restored image is insensitive to more than 20 iterations). The restored image is shown in Fig. 4, in which a jet-like feature (hereafter JLF) pointing to the north-east appears, in addition to the $\sim 30''$ diameter nebula coincident with the brightest radio region. The angular distance from the head of the JLF to the center of the central bright nebula is about $40''$. The total photon flux of the nebula is 2.07 10^{-2} counts s^{-1}, that of the JLF is about 3.9 10^{-3} counts s^{-1}; about 430 and 80 photons have been detected from the nebula proper and the JLF, respectively.

In order to examine the robustness of the restored image, we performed a Monte-Carlo simulation. Figure 5a displays an object which we assume to represent the basic morphology of G54.1+0.3 in shape and flux. Figure 5b is the simulated *ROSAT* PSPC observational result with the same observing time and background level as the real observation of G54.1+0.3, and Fig. 5c is a smoothed image of 5b. Figure 5d is the restored image of 5b. The close correspondance of the images shown in Figs. 5a and 5d demonstrates that the PSPC X-ray image of G54.1+0.3 is consistent with the presence of a jet.

4. Discussion

4.1. Distance and X-ray luminosity of G54.1+0.3

Velusamy & Becker (1988) suggested that G54.1+0.3 may have a distance of about 3.2 kpc, if its progenitor is in the star-forming region G53.9+0.3. The galactic HI column density in this direction is about 14.5 10^{21} cm^{-2} (Dickey & Lockman 1990). The best fit column density we get from the *ROSAT* PSPC observation is a little lower and the best fit column density of the *ASCA* SIS observation is a little higher. The range of column densities implies a distance consistent with the extent of the Galaxy, a result similar to that obtained by Seward (1989). A distance of 10 kpc appears to be quite reasonable. The X-ray luminosity in the 0.7–10.0 keV band is $L_{\rm X} = 1.4\ 10^{35} d_{10}^2$ erg s^{-1}, where d_{10} is the distance in units of 10 kpc. Even for a distance as large as 10 kpc the X-ray luminosity of G54.1+0.3 is slightly more than two orders of magnitude lower than that of the Crab Nebula (Toor & Seward 1974), but close to that of G21.5-0.9 (Becker & Szymkowiak 1981), which is another, so far undisputed, plerionic remnant.

The radio luminosity $L_{\rm r}$ of G54.1+0.3 is about 5 10^{33} d_{10}^2 erg s^{-1}, derived from the radio observations of

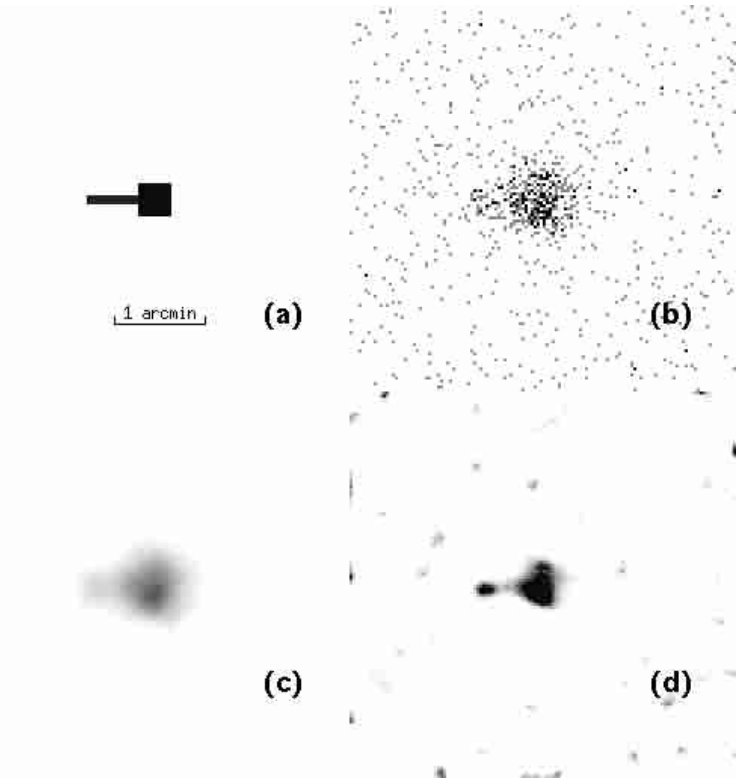

Fig. 5. Simulation of the *ROSAT* PSPC observation and image restoration to an object similar to G54.1+0.3. **a)** is an idealized object of similar shape and the same flux as G54.1+0.3. **b)** is the simulated *ROSAT* PSPC brightness map based on **a)** adopting the exposure time and background level of the observation. **c)** is image **b)** smoothed with a $10''$ $FWHM$ Gaussian filter. **d)** is the restored image of **b)**. Each of the four images displayed in **a)**–**d)** has the same angular scale as the images shown in Figs. 1 and 4. Note that any noisy features do not show up in **c)** because of the high cut level chosen

Velusamy & Becker (1988). The ratio $L_{\rm x}/L_{\rm r} = 28$, which is about a factor of 5 lower than that of the Crab but again similar to that of G21.5-0.9 (Helfand & Becker 1987).

Seward & Wang (1988) have shown that a relation between X-ray luminosity $L_{\rm X}$ of a plerionic SNR and rate of loss of rotational energy ($\dot{E}$) of the central pulsar appears to exist. Using their relation we derive $\dot{E} \sim 1.6\ 10^{37}$ erg s^{-1} for the central pulsar in G54.1+0.3.

4.2. Electron energy distribution

The *ASCA* SIS observation of G54.1+0.3 shows that the X-ray flux $F_{\rm x}$ at 1 keV is about $1.6\ 10^{-3}$ mJy. As the radio flux $F_{\rm r}$ at 1.4 GHz is 478 mJy, the flux spectral index between radio and X-ray is about -0.7, a little flatter than the *ASCA* SIS obtained X-ray energy index (-0.9) and much steeper than the radio spectral index $\alpha_{\rm r} = -0.13$ (Velusamy & Becker 1988), indicating that the spectrum contains a break between the radio and X-ray bands at a frequency around 10^{11} Hz.

If the relativistic electrons have a power law energy distribution $n_{\rm e} = E^{\gamma}$, the spectral index α is $\frac{\gamma+1}{2}$. The spectral break is associated with a similar break in the electron energy distribution. The synchrotron critical frequency of a relativistic electron of energy E in a magnetic field B is $\nu_{\rm c} = 16.1BE^2 \sin\psi$ MHz, where B is in μG, E is in GeV and ψ is the pitch angle (Lang 1998). Electrons with peak emission at 1 GHz have typical energies of $9.4B^{-0.5}$ GeV with B in μG and for a pitch angle of 45°. Similarly the X-ray (around 1 keV) emitting electrons have typical energies of $94B^{-0.5}$ TeV. If the magnetic field is about 10 μG the electron energy distribution is $\propto E^{-1.3}$ around 30 GeV and $\propto E^{-2.8}$ around 300 TeV. The spectral break occurs between 30 GeV and 300 TeV, probably around 300 GeV.

The lifetime of a relativistic electron against synchrotron losses can be represented by $t_{1/2}$, the time span over which the electron has lost half of its initial energy E_0; $t_{1/2} = \frac{8.35\ 10^9}{(B \sin\psi)^2 E_0}$ years, (Lang 1998). The lifetime of electrons radiating 30 GeV, 300 GeV or 300 TeV photons in a 10 μG field are about 5.6 10^6, 5.6 10^5, 5.6 10^2 years, respectively. These three typical lifetimes will be used in the discussion of the energy spectrum in the following section.

If the electrons from the putative central pulsar had initially a continuous power law energy distribution, the observed break would be due to the short lifetime of the high energy electrons. Because the low energy electrons which radiate at radio frequencies have a long lifetime, their energy distribution represents the initial electron energy distribution. The expected energy flux ratio $\frac{f_{1.4\ \rm GHz}}{f_{1\ \rm keV}}$ is then $\sim$11.8. The currently observed energy flux ratio $\frac{f_{1.4\ \rm GHz}}{f_{1\ \rm keV}}$ of 3.0 10^5 indicates that the age of G54.1+0.3 would be about $\frac{3.0\ 10^5}{11.8}$ $(-4\alpha_{\rm r})$ 5.6 10^2 years = 7.4 10^6 years. This large value for the apparent age suggests that the break in the energy spectrum is likely to be an intrinsic property of the putative pulsar. However, we note that the result is largely dependent on B; if B were as high as 500 μG as deduced for the Crab Nebula magnetic field, the time required to obtain the observed flux ratio between radio and X-ray emission for G54.1+0.3 would be just 3000 years, which is not unlikely given the small extent of the remnant of clearly less than $6\times d_{10}$ pc in diameter.

4.3. The X-ray jet

For the first time, a spatially resolved X-ray image of G54.1+0.3 has been obtained and an X-ray JLF pointing to the north-east has been detected. Simulations show that such a structure can in principle be observed by the *ROSAT* PSPC. The simulations also show that the JLF cannot be attributed to statistical fluctuations of the bright main source. We have also checked the time history of the photon events and the "wobble" direction of *ROSAT* during the observation, in order to see whether the JLF could have been produced by an accidental off-set in attitude or uncorrected "wobble" residuals. The time history file shows that the counts are distributed quite

smoothly in time with at most 6 counts detected in slots of 500 s, excluding a chance accumulation of counts at the JLF position. The "wobble" direction of *ROSAT* was along the south-east north-west line, which is nearly perpendicular to the JLF. Therefore we conclude that the JLF is due to a real X-ray source in the sky.

We have studied the possibility that the JLF is a separate object close to but not part of G54.1+0.3. We have not found any counterpart in the 30″ vicinity of the JLF except G54.1+0.3 itself. The optical plate obtained by Palomar Observatory Sky Survey and electronically reproduced by Skyview of NASA/GSFC does not show any source in the JLF region. The JLF reproduced in Fig. 5 indicates some brightness increase in the head area. It might be a false product of the restoration process because of the low number of counts, but we point out that some similar structure exists in the 4.8 GHz radio map. Additional simulations demonstrate that the length of the JLF is fairly well determined but the width of the JLF might have an uncertainty of up to ∼50%.

We have compared Fig. 4 with the 4.8 GHz VLA map obtained by Velusamy & Becker (1988) in detail. The brightest region of the nebula proper falls on $\alpha_{2000} = 19^{\rm h}30^{\rm m}30\overset{\rm s}{.}0$, $\delta_{2000} = 18°52'07''$, which coincides with the brightest region of the radio source. The head of the JLF is at $\alpha_{2000} = 19^{\rm h}30^{\rm m}32\overset{\rm s}{.}2$, $\delta_{2000} = 18°52'31''$, which also coincides with the north-eastern enhancement in the radio map. The positional coincidence of the X-ray and radio peaks strongly favors a common origin. The X-ray source has a smaller extent than the radio source and no significant X-ray emission has been detected along the northern radio feature, which was suggested to be the most probable radio JLF by Velusamy & Becker (1988). The lack of coincidence there might be due to the low sensitivity of the present observation.

Two ways to explain the origin of the X-ray JLF come to mind. The JLF might be the image of a fragment produced in the supernova explosion, like the fragments detected around the Vela SNR, especially the "bullet" – like fragment A (Aschenbach et al. 1995; Strom et al. 1995). But significant radio emission has only been detected around the head of the fragment, which implies that most of the relativistic electrons are contained in the leading edge of the fragment (Strom et al. 1995). In the case of G54.1+0.3 the radio surface brightness of the JLF follows the X-ray brightness, indicating a similar distribution of relativistic electrons responsible for the radio and X-ray emission. This makes a fragment-type origin of the X-ray JLF unlikely. An alternative interpretation is that the X-ray JLF is due to relativistic electrons produced and ejected by a central pulsar. Jets in pulsar-driven synchrotron nebulae have been detected in PSR 1929+10 (Wang et al. 1993), the Crab (Hester et al. 1995), the Vela SNR (Markwardt & Ögelman 1995), MSH 15-52 (Tamura et al. 1996), CTB80 (Wang & Seward 1984; Safi-Harb et al. 1995) and N157B in the Large Magellanic Cloud (Wang & Gotthelf 1998). In the case of the Vela pulsar jet (Frail et al. 1997) and N157B (Wang & Gotthelf 1998) both radio and X-ray emission have been observed from the respective jet.

The X-ray emission of the Vela pulsar jet can be fitted with both a power law and a thermally radiating plasma model (Markwardt & Ögelman 1995), whereas the X-ray pulsar jet in MSH15-52 appears to be nonthermal. We cannot derive the spectral properties of the X-ray jet in G54.1+0.3 with the present data. If we assume that the spectrum has the same power law shape as the entire remnant, the X-ray luminosity of the jet in the 0.1–2.4 keV band is about $2.1\ 10^{34} d_{10}^2\ {\rm erg\,s^{-1}}$.

From the radio map of Velusamy & Becker (1988) we estimate that the flux of the jet at 4.8 GHz is about 40 mJy. The X-ray flux at 1 keV is about $2.5\ 10^{-4}$ mJy. The two flux values give a spectral index bridging the radio and X-ray regimes of about −0.68, quite similar to that of the whole remnant. As no significant radio spectral variation across the source has been detected (Velusamy & Becker 1988), the jet electrons are likely to have a break in the energy distribution similar to that of the whole remnant.

The distance of the jet head to the nebula center is about 40″. It corresponds to 2 pc if the SNR is 10 kpc away. Recent distance measurements of the Vela SNR suggest a distance of 250 ± 30 pc (Cha et al. 1999), which implies that the Vela pulsar jet is about 3 pc long (Cha et al. 1999; Markwardt & Ögelman 1995). The lengths of the two jets appear to be quite similar.

5. Summary

The *ROSAT* PSPC and the *ASCA* spectra imply a large distance of G54.1+0.5 comparable with the galactic radius. The X-ray spectrum is clearly nonthermal. The comparison of the radio and X-ray flux levels shows that the energy distribution of the relativistic electrons has a break, which is around 300 GeV for a magnetic field of about 10 μG. For this low value of B the break is quite probably an intrinsic property of the relativistic electron spectrum of a central pulsar rather than the effect of strong synchrotron losses, because in the latter case the remnant should be as old as $7.4\ 10^6$ years. But such an age is in contrast to the rather small diameter of G54.1+0.3, which implies a much younger remnant. For $B \approx 500\ \mu$G, as in the Crab Nebula, the age is about 3000 years, compatible with the linear diameter, and the steepening of the photon spectrum could be attributed to synchrotron losses impacting on a single power law electron energy spectrum.

The deconvolution of the *ROSAT* PSPC image shows an X-ray jet pointing towards the north-east, which also shows up in the radio image. The non-thermal spectrum confirms the classification of G54.1+0.3 as a Crab-like SNR, although no pulsations have been found in the X-ray observation. Future deep X-ray observations with high spatial and spectral resolution available with the Chandra and XMM-Newton observatories will help to clarify the spectral and spatial structure of the remnant as well as the X-ray jet.

Acknowledgements. F. J. Lu is supported by the exchange program between the Max-Planck Society and the Chinese Academy of Sciences. He thanks Professor J. Trümper for hospitality. The authors thank Drs. S. D. Mao and Q. D. Wang for helpful discussions. This research is partially supported by the Special Funds for Major State Basic Research Projects and the National Natural Science Foundation of China. Both the SIMBAD database, operated at CDS, Strasbourg, France and the Digitized Sky Survey operated by Skyview of NASA/GSFC were used for this research.

References

Angerhofer, P. E., Strom, R. G., Velusamy, T., et al. 1981, A&A, 94, 313
Aschenbach, B., Egger, R., & Trümper, J. 1995, Nature, 373, 587
Becker, R. H., & Szymkowiak, A. E. 1981, ApJ, 248, L23
Cha, A. N., Sembach, K. R., & Danks, A. C. 1999, ApJ, 515, L25
Dickey, J. M., & Lockman, F. J. 1990, ARA&A, 28, 215
Frail, D. A., Bietenholz, M. F., & Markwardt, C. B., et al. 1997, ApJ, 475, 224
Helfand, D. J., & Becker, R. H. 1987, ApJ, 314, 203
Hester, J. J., Scowen, P. A., Sankrit, R., et al. 1995, ApJ, 448, 240
Lang, K. R. 1998, Astrophysical Formulae (Springer)
Li, T. P., & Wu, M. 1994, Ap&SS, 215, 213
Lu, F. J., Li, T. P., Sun, X. J., et al. 1996, A&AS, 115, 395
Lucy, L. 1974, AJ, 79, 745
Markwardt, C. B., & Ögelman H. 1995, Nature, 375, 40
Raymond, J. C., & Smith, B. W. 1977, ApJS, 35, 419
Reich, W., Fürst, E., Altenhoff, W. J., et al. 1985, A&A, 151, L10
Richardson, B. M. 1972, J. Opt. Soc. Am., 62, 55
Roger, R. S., Milne, D. K., Kesteven, M. J., et al. 1985, Nature, 316, 44
Safi-Harb, S., Ögelman, H., & Finley, J. P. 1995, ApJ, 439, 722
Seward, F. D. 1989, AJ, 97, 481
Seward, F. D., & Wang, Z. R. 1988, ApJ, 332, 199
Strom, R., Johnston, H. M., Verbunt, F., et al. 1995, Nature, 373, 590
Tamura, K., Kawai, N., Yoshida, A., et al. 1996, PASJ, 48, L33
Tanaka, Y., Inoue, H., & Holt, S. S. 1994, PASJ, 46, L37
Toor, A., & Seward, F. D. 1974, AJ, 79, 995
Velusamy, T. 1984, Nature, 308, 15
Velusamy, T., & Becker, R. H. 1988, AJ, 95, 1162
Wang, Q. D., & Gotthelf, E. V. 1998, ApJ, 494, 623
Wang, Q. D., Li, Z. Y., & Begelman, M. C. 1993, Nature, 364, 127
Wang, Z. R., & Seward, F. D. 1984, ApJ, 285, 607
Zhang, S., Li, T. P., & Wu, M. 1998, A&A, 340, 62
Zimmermann, U., Boese, G., Becker, W., et al. 1998, EXSAS user's guide, MPE Report